Steel and Composite Structures, *Vol. 22, No. 4 (2016) 889-913*
DOI: http://dx.doi.org/10.12989/scs.2016.22.4.889

Differential cubature method for vibration analysis of embedded FG-CNT-reinforced piezoelectric cylindrical shells subjected to uniform and non-uniform temperature distributions

Hamid Madani [1], Hadi Hosseini [2] and Maryam Shokravi*[3]

[1] *Young Researcher and Elite Club, Jasb Branch, Islamic Azad University, Jasb, Iran*
[2] *Department of Civil Engineering, Khomein Branch, Islamic Azad University, Khomein, Iran*
[3] *Buein Zahra Technical University, Buein Zahra, Qazvin, Iran*

(*Received June 28, 2016, Revised October 16, 2016, Accepted November 04, 2016*)

Abstract. Vibration analysis of embedded functionally graded (FG)-carbon nanotubes (CNT)-reinforced piezoelectric cylindrical shell subjected to uniform and non-uniform temperature distributions are presented. The structure is subjected to an applied voltage in thickness direction which operates in control of vibration behavior of system. The CNT reinforcement is either uniformly distributed or functionally graded (FG) along the thickness direction indicated with FGV, FGO and FGX. Effective properties of nano-composite structure are estimated through Mixture low. The surrounding elastic foundation is simulated with spring and shear constants. The material properties of shell and elastic medium constants are assumed temperature-dependent. The motion equations are derived using Hamilton's principle applying first order shear deformation theory (FSDT). Based on differential cubature (DC) method, the frequency of nano-composite structure is obtained for different boundary conditions. A detailed parametric study is conducted to elucidate the influences of external applied voltage, elastic medium type, temperature distribution type, boundary conditions, volume percent and distribution type of CNT are shown on the frequency of system. In addition, the mode shapes of shell for the first and second modes are presented for different boundary conditions. Numerical results indicate that applying negative voltage yields to higher frequency. In addition, FGX distribution of CNT is better than other considered cases.

Keywords: vibration of piezoelectric shell; FG-CNT; DC method; Non-uniform temperature distribution; temperature-dependent

1. Introduction

A great deal of interest for the analysis of carbon nanotube-reinforced composite (CNTRC) structures is being manifested in the specialized literature. This interest is mainly due to the advent of the new composite material systems exhibiting exotic properties as compared to the traditional, carbon fiber-reinforced composite structures. Due to their very attractive thermo-mechanical properties these new materials are going to play a great role in the construction of Micro-Electro-Mechanical Systems (MEMS) and Nano-Electro-Mechanical Systems (NEMS).

Functionally graded materials (FGMs) have found a wide range of applications in many

*Corresponding author, Ph.D., E-mail: Maryamshokravi10@yahoo.com; Maryamshokravi10@bzte.ac.ir

http://www.techno-press.org/?journal=scs&subpage=6 ISSN: 1229-9367 (Print), 1598-6233 (Online)

industries. Rajesh Bhangale and Ganesan (2005) investigated free vibration of non-homogeneous FG magneto- electro-elastic finite cylindrical shells with simply supported boundary condition. Based on differential quadrature method, static analysis of FG cylindrical shell integrated with piezoelectric layers was analyzed by Alibeigloo and Nouri (2010). Sheng and Wang (2009a, b, 2010) investigated active vibration control, displacements and buckling of FG laminated cylindrical shells integrated with piezoelectric layers. Based on an analytical approach, the free vibration and transient response of FG piezoelectric cylindrical panels subjected to impulsive loads were presented by Bodaghi and Shakeri (2012). The mechanical and thermal buckling behaviors of ceramic–metal functionally grade plates (FGPs) were studied by Zhang *et al*. (2014c) using a local Kriging meshless method. The local meshless method was developed based on the local Petrov–Galerkin weak-form formulation combined with shape functions having the Kronecker delta function property, constructed by the Kriging interpolation. Based on the proposed method by Zhang *et al*. (2014a), geometrically nonlinear thermoelastic analysis of FGM plates in thermal environments was developed by Zhu *et al*. (2014). In the thermal analysis, the dependency of thermal conductivity of functionally graded materials on temperature was involved, which gives rise to a nonlinear partial differential heat conduction equation. Zhang *et al*. (2015a) investigated active vibration control of piezoelectric bonded smart structures using PID algorithm. A nonlinear deflection analysis was carried out by Zhang and Liew (2016a) for internal column supported functionally graded material (FGM) arbitrarily straight-sided quadrilateral plates under a uniformly distributed loading based on based on the element-free IMLS-Ritz method. Noted that the mentioned method was used by Zhang *et al*. (2015a, b) for solution of elastodynamic problems and three-dimensional wave equations. Postbuckling behavior of biaxial compressed straight-sided, functionally graded material (FGM) plates of quadrilateral shape was studied by Zhang *et al*. (2016a) using the IMLS-Ritz method and first-order shear deformation theory (FSDT) with the von Kármán nonlinearity.

None of the above researchers have considered nanocomposite structures. The traditional approach to fabricating nanocomposites implies that the nanotube is distributed either uniformly or randomly such that the resulting mechanical, thermal, or physical properties do not vary spatially at the macroscopic level. Functionally graded materials (FGMs) are a new generation of composite materials in which the micro-structural details are spatially varied through non-uniform distribution of the reinforcement phase. Static analysis of functionally graded carbon nanotube (FG-CNT) reinforced composite plate imbedded in piezoelectric layers was discussed by Alibeigloo (2013). A first attempt to use the mesh-free kp-Ritz method for large deflection geometrically nonlinear analysis of carbon nanotube-reinforced functionally graded (CNTR-FG) cylindrical panels subjected to mechanical loads was performed by Zhang *et al*. (2014b). The mesh-free kp-Ritz was utilized by Lei *et al*. (2014) for dynamic stability analysis of CNTR-FG cylindrical panels under static and periodic axial force. Based on FSDT, Zhang *et al*. (2014c) employed the mesh-free kp-Ritz for analysis of flexural strength and free vibration of FG-CNTRC cylindrical panels. Liew *et al*. (2014) analyzed postbuckling of various types of CNTR-FG cylindrical panels, using the element-free kp-Ritz method combined with the FSDT and von Kármán strains. Zhang *et al*. (2015c) reported free vibration analysis of FG-CNT reinforced triangular plates using the FSDT and element-free IMLS-Ritz method. The vibration behaviors of functionally graded carbon nanotube (FG-CNT) reinforced composite rectangular plates subjected to in-plane loads were studied by Zhang *et al*. (2015d). Based on state-space Levy method, the critical in-plane loads for the buckling of different FG-CNT plates were calculated and compared. The geometrically nonlinear large deformation and buckling analysis of FG-CNT reinforced

composite skew plates resting on Pasternak foundations was presented by Zhang and Liew (2015a) and Zhang *et al*. (2015e). Parametric studies were conducted to examine the effects of CNT content by volume, elastic foundation, skew angle, plate width-to-thickness ratio, plate aspect ratio and boundary conditions on the nonlinear responses of the FG-CNT reinforced composite skew plates. Nonlinear bending behaviors of FG-CNT reinforced composite thick plates were presented by Zhang *et al*. (2015f) based on arc-length iterative algorithm and the modified Newton–Raphson method. Free vibration of FG-CNT reinforced composite moderately thick rectangular plates with edges elastically restrained against transverse displacements and rotation of the plate cross section was considered by Zhang *et al*. (2015g). They used FSDT for modeling of structure and element-free improved moving least-squares Ritz (IMLS-Ritz) method for solution. Based on FSDT, Lei *et al*. (2015a, b) presented the vibration and Elastodynamic analysis of laminated FG-CNT reinforced composite rectangular plates and carbon nanotube-reinforced functionally graded (CNTR-FG) plates using the element-free kp-Ritz method. Numerical simulations were used to study the effect of carbon nanotube volume fraction, plate width-to-thickness ratio, plate aspect ratio, boundary condition, load type and distribution type of carbon nanotubes on the dynamic responses of structure. An improved moving least-squares (IMLS) approximation for the field variables was proposed by Zhang and Liew (2015b) for geometrically nonlinear large deformation analysis of FG-CNT reinforced composite quadrilateral plates. The modified Newton–Raphson method combined with the arc-length iterative algorithm was employed to solve the nonlinear deformation of the structure. Lei *et al*. (2016) investigated bending responses of laminated carbon nanotube-reinforced functionally graded composite plates. Effective material properties of the laminated nanocomposite plates were estimated using the extended rule of mixture. Zhang *et al*. (2016a) presented a geometrically nonlinear analysis of carbon nanotube reinforced functionally graded composite plates with elastically restrained edges and internal supports. The governing equation to this problem was derived through the IMLS-Ritz method. Zhang *et al*. (2016b, c, d) studied postbuckling analysis of carbon nanotube reinforced functionally graded plates with edges elastically restrained against translation and rotation, FG-CNT reinforced composite plates resting on Pasternak foundations and laminated nanocomposite plates subjected to biaxial and uniaxial compression. In the mentioned works, the IMLS-Ritz method was used. An aerothermoelastic analysis of carbon nanotube reinforced functionally graded composite panels in supersonic airflow was presented by Zhang *et al*. (2016e) based on Reddy's third-order shear deformation theory. Meanwhile, the active flutter control of CNT reinforced functionally graded composite panels was also carried out using the piezoelectric actuator and sensor. Optimal shape control of CNT reinforced functionally graded composite plates was studied by Zhang *et al*. (2016f) based on genetic algorithm. The effects of CNT distributions and plate aspect ratios on optimal shape control results were investigated. Utilizing the FSDT element-free method, Zhang *et al*. (2016g, 2016h) investigated elastodynamic and free vibration analysis of quadrilateral and triangular CNT-reinforced composite plates. Detailed numerical simulations were carried out to investigate the effect of CNT volume fraction, CNT distribution type, side angles, area of quadrilateral plate, isosceles triangular angle, plate width-to-thickness ratio and boundary condition on the dynamic behaviors of structure.

However, to date, no report has been found in the literature on vibration analysis of FG-CNT-reinforced piezoelectric cylindrical shell subjected to non-uniform temperate distribution. Motivated by these considerations, in the present study, temperature-dependent vibration analysis of embedded FG-CNT-reinforced piezoelectric cylindrical shell is investigated. The structure is subjected to external applied voltage, uniform and non-uniform temperate distributions. The rule

of mixture is used for calculating the equivalent material properties of nano-composite structure. The surrounding elastic medium is simulated by Pasternak foundation. The motion equations are derived based on FSDT in conjunction with Hamilton's principal. The frequency of structure is obtained using DC method for different boundary conditions. The effects of applied voltage, volume percent and distribution type of CNT in polymer, temperature distribution type, elastic medium and boundary conditions on the frequency of system are disused in detail.

2. FSDT theory

Based on FSDT shell theory, the displacement field can be expressed as (Reddy 2002)

$$u\left(x,\theta,z,t\right)=u\left(x,\theta,t\right)+z\phi_x\left(x,\theta,t\right), \tag{1a}$$

$$v\left(x,\theta,z,t\right)=v\left(x,\theta,t\right)+z\phi_\theta\left(x,\theta,t\right), \tag{1b}$$

$$w\left(x,\theta,z,t\right)=w\left(x,\theta,t\right), \tag{1c}$$

where ($u(x, \theta, z, t)$, $v(x, \theta, z, t)$, $w(x, \theta, z, t)$) denote the displacement components at an arbitrary point (x, θ, z) in the shell, and ($u(x, \theta, t)$, $v(x, \theta, t)$, $w(x, \theta, t)$) are the displacement of a material point at (x, θ) on the mid-plane (i.e., z = 0) of the shell along the x-, θ-, and z-directions, respectively; ϕ_x and ϕ_θ are the rotations of the normal to the mid-plane about x- and θ- directions, respectively. Based on above relations, the strain-displacement equations may be written as

$$\varepsilon_{xx}=\frac{\partial u}{\partial x}+z\frac{\partial \phi_x}{\partial x}, \tag{2a}$$

$$\varepsilon_{\theta\theta}=\frac{1}{R}\left(w+\frac{\partial v}{\partial \theta}\right)+\frac{z}{R}\frac{\partial \phi_\theta}{\partial \theta}, \tag{2b}$$

$$\gamma_{x\theta}=\frac{\partial v}{\partial x}+\frac{1}{R}\left(\frac{\partial u}{\partial \theta}\right)+z\left(\frac{\partial \phi_\theta}{\partial x}+\frac{1}{R}\frac{\partial \phi_x}{\partial \theta}\right), \tag{2c}$$

$$\gamma_{xz}=\phi_x+\frac{\partial w}{\partial x}, \tag{2d}$$

$$\gamma_{z\theta}=\frac{1}{R}\left(\frac{\partial w}{\partial \theta}-v\right)+\phi_\theta. \tag{2e}$$

where (ε_{xx}, $\varepsilon_{\theta\theta}$) are the normal strain components and ($\gamma_{\theta z}$, γ_{xz}, $\gamma_{x\theta}$) are the shear strain components.

3. Constitutive equations of piezoelectric material

The subsequent characterization of electromechanical coupling covers the various classes of

piezoelectric materials. Details with respect to definition and determination of the constants describing these materials have been standardized by the Institute of Electrical and Electronics Engineers (Alibeigloo,2013). Stresses σ and strains ε on the mechanical side, as well as flux density D and field strength E on the electrostatic side, may be arbitrarily combined as follows (Tiersten 1969)

$$\begin{bmatrix}\sigma_{xx}\\ \sigma_{\theta\theta}\\ \sigma_{zz}\\ \tau_{\theta z}\\ \tau_{xz}\\ \tau_{x\theta}\end{bmatrix}=\begin{bmatrix}C_{11} & C_{12} & C_{13} & 0 & 0 & 0\\ C_{12} & C_{22} & C_{23} & 0 & 0 & 0\\ C_{13} & C_{23} & C_{33} & 0 & 0 & 0\\ 0 & 0 & 0 & C_{44} & 0 & 0\\ 0 & 0 & 0 & 0 & C_{55} & 0\\ 0 & 0 & 0 & 0 & 0 & C_{66}\end{bmatrix}\left(\begin{Bmatrix}\varepsilon_{xx}-\alpha_{xx}\Delta T\\ \varepsilon_{\theta\theta}-\alpha_{\theta\theta}\Delta T\\ \varepsilon_{zz}-\alpha_{zz}\Delta T\\ \gamma_{\theta z}\\ \gamma_{xz}\\ \gamma_{x\theta}\end{Bmatrix}\right)-\begin{bmatrix}0 & 0 & e_{31}\\ 0 & 0 & e_{32}\\ 0 & 0 & e_{33}\\ 0 & e_{24} & 0\\ e_{15} & 0 & 0\\ 0 & 0 & 0\end{bmatrix}\begin{Bmatrix}E_x\\ E_\theta\\ E_z\end{Bmatrix} \tag{3}$$

$$\begin{bmatrix}D_x\\ D_\theta\\ D_z\end{bmatrix}=\begin{bmatrix}0 & 0 & 0 & 0 & e_{15} & 0\\ 0 & 0 & 0 & e_{24} & 0 & 0\\ e_{31} & e_{31} & e_{33} & 0 & 0 & 0\end{bmatrix}\left(\begin{Bmatrix}\varepsilon_{xx}-\alpha_{xx}\Delta T\\ \varepsilon_{\theta\theta}-\alpha_{\theta\theta}\Delta T\\ \varepsilon_{zz}-\alpha_{zz}\Delta T\\ \gamma_{\theta z}\\ \gamma_{xz}\\ \gamma_{x\theta}\end{Bmatrix}\right)+\begin{bmatrix}\in_{11} & 0 & 0\\ 0 & \in_{22} & 0\\ 0 & 0 & \in_{33}\end{bmatrix}\begin{Bmatrix}E_x\\ E_\theta\\ E_z\end{Bmatrix} \tag{4}$$

where σ_{ij} ($i, j = x, \theta, z$), ε_{ij} ($i, j = x, \theta, z$), D_{ii} ($i = x, \theta, z$) and E_{ii} ($i = x, \theta, z$) are stress, strain, electric displacement and electric field, respectively. Also, Q_{ij} ($i, j = 1, 2,..., 6$), e_{ij} ($i, j = 1, 3, 4, 5$) and $\in_{ij}$ ($i, j = 1, 2, 3$) denote elastic, piezoelectric and dielectric coefficients, respectively. Noted that C_{ij} ($i, j = 1, 2,..., 6$) and α_{xx}, $\alpha_{\theta\theta}$ may be obtained using rule of mixture (next section). The electric field in terms of electric potential (Φ) is expressed as

$$E_k = -\nabla\Phi, \tag{5}$$

where, the electric potential is assumed as the combination of a half-cosine and linear variation, which satisfies the Maxwell equation. It can be written as (Liu *et al*. 2013)

$$\Phi(x,\theta,z,t) = -\cos(\frac{\pi z}{h})\phi(x,\theta,t)+\frac{2V_0 z}{h}, \tag{6}$$

where ϕ (x, θ, t) is the time and spatial distribution of the electric potential which must satisfy the electric boundary conditions, V_0 is external electric voltage.

However, using Eq. (1), the governing equations of piezoelectric material (i.e., Eqs. (3) and (4)) for FSDT may be written as

$$\sigma_{xx} = C_{11}\left(\varepsilon_{xx}-\alpha_{xx}\Delta T\right)+C_{12}\left(\varepsilon_{\theta\theta}-\alpha_{\theta\theta}\Delta T\right)+e_{31}\left(\frac{\pi}{h}\sin\left(\frac{\pi z}{h}\right)\varphi+\frac{2V_0}{h}\right), \tag{7}$$

$$\sigma_{\theta\theta} = C_{12}\left(\varepsilon_{xx}-\alpha_{xx}\Delta T\right)+C_{22}\left(\varepsilon_{\theta\theta}-\alpha_{\theta\theta}\Delta T\right)+e_{32}\left(\frac{\pi}{h}\sin\left(\frac{\pi z}{h}\right)\varphi+\frac{2V_0}{h}\right), \tag{8}$$

$$\sigma_{\theta z} = C_{44}\varepsilon_{\theta z} - e_{15}\left(\cos\left(\frac{\pi z}{h}\right)\frac{\partial\varphi}{R\partial\theta}\right), \tag{9}$$

$$\sigma_{zx} = C_{55}\varepsilon_{zx} - e_{24}\left(\cos\left(\frac{\pi z}{h}\right)\frac{\partial\varphi}{\partial x}\right), \tag{10}$$

$$\sigma_{x\theta} = C_{66}\gamma_{x\theta}, \tag{11}$$

$$D_x = e_{15}\varepsilon_{xz} + \in_{11}\left(\cos\left(\frac{\pi z}{h}\right)\frac{\partial\varphi}{R\partial\theta}\right), \tag{12}$$

$$D_\theta = e_{24}\varepsilon_{z\theta} + \in_{22}\left(\cos\left(\frac{\pi z}{h}\right)\frac{\partial\varphi}{R\partial\theta}\right), \tag{13}$$

$$D_x = e_{31}\varepsilon_{xx} + e_{32}\varepsilon_{\theta\theta} - \in_{33}\left(\frac{\pi}{h}\sin\left(\frac{\pi z}{h}\right)\varphi + \frac{2V_0}{h}\right). \tag{14}$$

4. Uniform and nano-uniform temperature distribution

In order to accurately describe the effect of the temperature rise through-the-thickness different temperature distributions are taken into account in the present analysis.

4.1 Uniform temperature rise

The cylindrical shell initial temperature is assumed to be T_i. The temperature is uniformly raised to a final value T. The temperature change is give by

$$\Delta T = T - T_i, \tag{15}$$

4.2 Linear temperature rise

The temperature of the outer surface is T_o and it is considered to vary linearly from T_t to the inner surface temperature T_i. Therefore, the temperature rise through-the-thickness is given by

$$T(\mathrm{z}) = \Delta T\left(\frac{z}{h} + \frac{1}{2}\right) + T_i, \qquad \Delta T = T_o - T_i. \tag{16}$$

4.3 Harmonic temperature rise

In the third case, the temperature distribution across the thickness direction follows a sinusoidal law as

$$T(z)=\Delta T\left(1-\cos\left[\frac{\pi}{2}\left(\frac{z}{h}+\frac{1}{2}\right)\right]\right)+T_i, \qquad \Delta T=T_o-T_i. \tag{17}$$

5. Mixture rule

As shown in Fig. 1, a FG-CNT reinforced piezoelectric cylindrical shell with length L and thickness h is considered. The structure is surrounded by Pasternak medium. One uniform and three functionally graded CNT distributions are considered. However, for calculating the equivalent material properties of present nano-composite structure, the rule of Mixture is applied.

According to this theory, the effective Young and shear moduli of structure may be expressed as (Liew *et al*. 2014, Zhang *et al*. 2015h)

$$E_{11}=\eta_1 V_{CNT}E_{r11}+(1-V_{CNT})E_m, \tag{18}$$

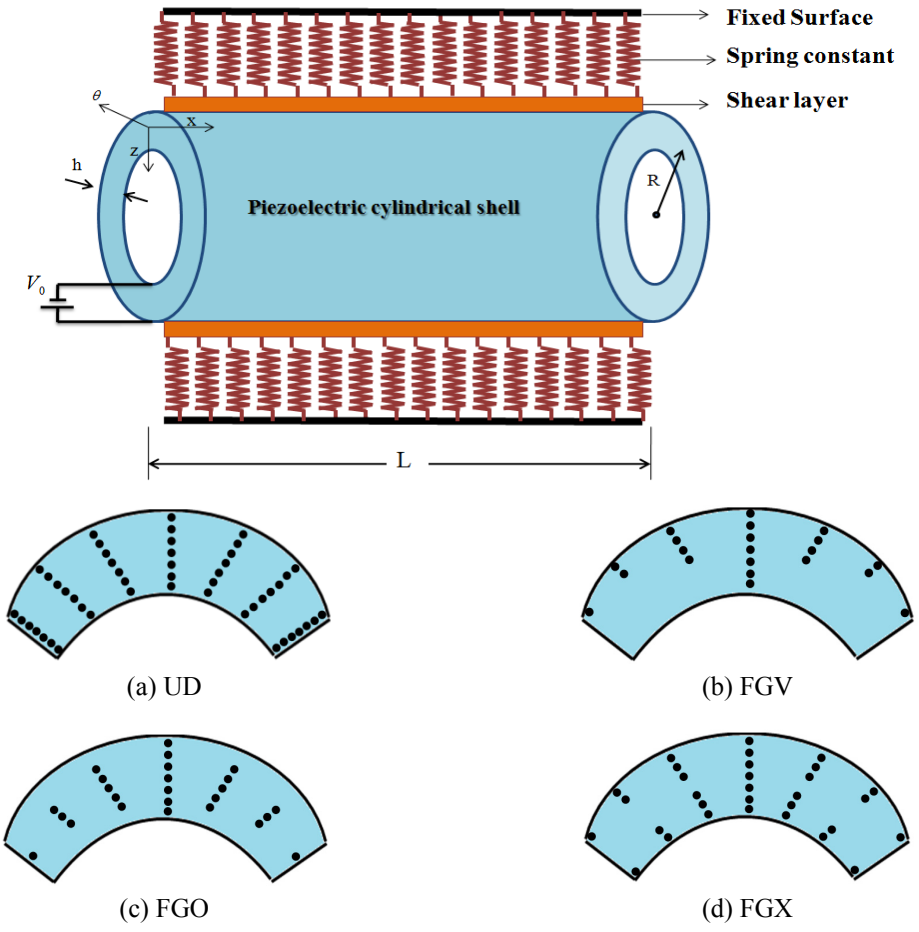

Fig. 1 Configurations of the CNT distribution in a piezoelectric cylindrical shell

$$\frac{\eta_2}{E_{22}}=\frac{V_{CNT}}{E_{r22}}+\frac{(1-V_{CNT})}{E_m}, \tag{19}$$

$$\frac{\eta_3}{G_{12}}=\frac{V_{CNT}}{G_{r12}}+\frac{(1-V_{CNT})}{G_m}, \tag{20}$$

where E_{r11}, E_{r22} and E_m are Young's moduli of CNTs and matrix, respectively; G_{r11} and G_m are shear modulus of CNTs and matrix, respectively; V_{CNT} and V_m show the volume fractions of the CNTs and matrix, respectively; η_j (j = 1, 2, 3) is CNT efficiency parameter for considering the size-dependent material properties. Noted that this parameter may be calculated using molecular dynamic (MD). However, the CNT distribution for the mentioned patters obeys from the following relations (Zhang *et al*. 2015h, Liew *et al*. 2014)

$$UD:\quad V_{CNT}=V_{CNT}^{*}, \tag{21a}$$

$$FGV:\quad V_{CNT}(z)=\left(1+\frac{2z}{h}\right)V_{CNT}^{*}, \tag{21b}$$

$$FGO:\quad V_{CNT}(z)=2\left(1-\frac{2|z|}{h}\right)V_{CNT}^{*}, \tag{21c}$$

$$FGX:\quad V_{CNT}(z)=2\left(\frac{2|z|}{h}\right)V_{CNT}^{*}, \tag{21d}$$

Furthermore, the thermal expansion coefficients in the axial and transverse directions respectively (α_{11} and α_{22}) and the density (ρ) of the nano-composite structure can be written as (Liew *et al*. 2014)

$$\rho=V_{CNT}\rho_r+V_{m,}\rho_{m,}, \tag{22a}$$

$$\alpha_{11}=V_{CNT}\alpha_{r11}+V_{m,}\alpha_{m,}, \tag{22b}$$

$$\alpha_{22}=\left(1+\nu_{r12}\right)V_{CNT}\alpha_{r22}+\left(1+\nu_m\right)V_m\alpha_m-\nu_{12}\alpha_{11}, \tag{22c}$$

where

$$V_{CNT}^{*}=\frac{w_{CNT}}{w_{CNT}+\left(\rho_{CNT}/\rho_m\right)-\left(\rho_{CNT}/\rho_m\right)w_{CNT}}, \tag{23}$$

where w_{CNT} is the mass fraction of the CNT; ρ_m and ρ_{CNT} present the densities of the matrix and CNT, respectively; ν_{r12} and ν_m are Poisson's ratios of the CNT and matrix, respectively; α_{r11}, α_{r22} and α_m are the thermal expansion coefficients of the CNT and matrix, respectively. Noted that ν_{12} is assumed as constant.

6. Energy method

The total potential energy, V, of the system is the sum of potential energy, U, kinetic energy, K, and the work done by the elastic medium, W.

6.1 Potential energy

The potential energy can be written as

$$U = \frac{1}{2}\int\left(\begin{matrix}\sigma_{xx}\varepsilon_{xx}+\sigma_{\theta\theta}\varepsilon_{\theta\theta}+\sigma_{xz}\varepsilon_{xz}+\sigma_{\theta z}\varepsilon_{\theta z}+\sigma_{x\theta}\gamma_{x\theta}\\ -D_x E_x - D_\theta E_\theta - D_z E_z\end{matrix}\right)dV\,, \tag{24}$$

Combining of Eqs. (1), (7)-(14) and (24) yields

$$\begin{aligned} U = \frac{1}{2}\int_0^{2\pi}\int_0^L \Bigg\{ & \left[N_{xx}\frac{\partial u}{\partial x}+M_{xx}\frac{\partial \phi_x}{\partial x}\right]+\left[\frac{N_{\theta\theta}}{R}\left(w+\frac{\partial v}{\partial \theta}\right)+\frac{M_{\theta\theta}}{R}\frac{\partial \phi_\theta}{\partial \theta}\right]+Q_x\left(\phi_x+\frac{\partial w}{\partial x}\right) \\ & +\left(N_{x\theta}\left[\frac{\partial v}{\partial x}+\frac{1}{R}\frac{\partial u}{\partial \theta}\right]+M_{x\theta}\left[\frac{\partial \phi_\theta}{\partial x}+\frac{1}{R}\frac{\partial \phi_x}{\partial \theta}\right]\right)+Q_\theta\left[\frac{1}{R}\left(\frac{\partial w}{\partial \theta}-v\right)+\phi_\theta\right]\Bigg\} R\,dx\,d\theta \\ \int_{-h/2}^{h/2}\int_0^{2\pi}\int_0^L & \left\{-D_x\left[\cos\left(\frac{\pi z}{h}\right)\frac{\partial \varphi}{\partial x}\right]-D_\theta\left[\cos\left(\frac{\pi z}{h}\right)\frac{\partial \varphi}{R\partial \theta}\right]-D_z\left[-\frac{\pi}{h}\sin\left(\frac{\pi z}{h}\right)\varphi-\frac{2V_0}{h}\right]\right\} R\,dx\,d\theta\,dz, \end{aligned} \tag{25}$$

where the stress resultant-displacement relations can be written as

$$\begin{Bmatrix} N_{xx}\\ N_{\theta\theta}\\ N_{x\theta}\end{Bmatrix} = \int_{-\frac{h}{2}}^{\frac{h}{2}}\begin{Bmatrix}\sigma_{xx}\\ \sigma_{\theta\theta}\\ \tau_{x\theta}\end{Bmatrix}dz \tag{26}$$

$$\begin{Bmatrix} Q_x\\ Q_\theta\end{Bmatrix} = k'\int_{-\frac{h}{2}}^{\frac{h}{2}}\begin{Bmatrix}\sigma_{xz}\\ \sigma_{\theta z}\end{Bmatrix}dz \tag{27}$$

$$\begin{Bmatrix} M_{xx}\\ M_{\theta\theta}\\ M_{x\theta}\end{Bmatrix} = \int_{-\frac{h}{2}}^{\frac{h}{2}}\begin{Bmatrix}\sigma_{xx}\\ \sigma_{\theta\theta}\\ \tau_{x\theta}\end{Bmatrix}z\,dz \tag{28}$$

In which k' is shear correction coefficient. Substituting Eqs. (1) and (7)-(14) into Eqs. (26)-(28), the stress resultant-displacement relations can be obtained as reported in Appendix A.

6.2 Kinetic energy

The kinetic energy of system may be written as

$$K=\frac{\rho}{2}\int\left(\left(\frac{\partial u}{\partial t}+z\frac{\partial \phi_x}{\partial t}\right)^2+\left(\frac{\partial v}{\partial t}+z\frac{\partial \phi_\theta}{\partial t}\right)^2+\left(\frac{\partial w}{\partial t}\right)^2\right)dV. \tag{29}$$

Defining the moments of inertia as below

$$\begin{Bmatrix} I_0 \\ I_1 \\ I_2 \end{Bmatrix}=\int_{z^{(k-1)}}^{z^{(k)}}\begin{bmatrix} \rho \\ \rho z \\ \rho z^2 \end{bmatrix}dz, \tag{30}$$

the kinetic energy may be written as

$$K=\frac{1}{2}\int\begin{pmatrix} I_0\left(\left(\frac{\partial u}{\partial t}\right)^2+\left(\frac{\partial v}{\partial t}\right)^2+\left(\frac{\partial w}{\partial t}\right)^2\right)+I_1\left(2\frac{\partial u}{\partial t}\frac{\partial \phi_x}{\partial t}+2\frac{\partial v}{\partial t}\frac{\partial \phi_\theta}{\partial t}\right) \\ +I_2\left(\left(\frac{\partial \phi_x}{\partial t}\right)^2+\left(\frac{\partial \phi_\theta}{\partial t}\right)^2\right)\end{pmatrix}dA, \tag{31}$$

6.3 External works

The external work due to Pasternak medium can be written as (Shen and Chen 2011)

$$W_e=\int_0^{2\pi}\int_0^{L}\left(-K_w w+K_g\nabla^2 w\right)dA, \tag{32}$$

where K_w and K_g are Winkler's spring modulus and shear layer coefficients, respectively. The foundation stiffness K_w for soft medium may be written by

$$K_w=\frac{E_0}{4L(1-\nu_0^2)(2-c_1)^2}\left[5-\left(2\gamma_1^2+6\gamma_1+5\right)\exp\left(-2\gamma_1\right)\right], \tag{33}$$

where

$$c_1=\left(\gamma_1+2\right)\exp\left(-\gamma_1\right), \tag{34a}$$

$$\gamma_1=\frac{H_s}{L}, \tag{34b}$$

$$E_0=\frac{E_s}{\left(1-\nu_s^2\right)}, \tag{34c}$$

$$\nu_0=\frac{\nu_s}{\left(1-\nu_s\right)}, \tag{34d}$$

where E_s, v_s, H_s are Young's modulus, Poisson's ratio and depth of the foundation, respectively. In this paper, E_s is assumed to be temperature-dependent while v_s is assumed to be a constant. In addition, the in-plane forces may be written as

$$W = -\frac{1}{2}\int\left[N_{xx}^{f}\left(\frac{\partial w}{\partial x}\right)^2 + \frac{N_{\theta\theta}^{f}}{R^2}\left(\frac{\partial w}{\partial y}\right)^2\right] R dx d\theta, \tag{35}$$

where

$$N_{xx}^{f} = N_{xx}^{M} + N_{xx}^{T} + N_{xx}^{E}, \tag{36}$$

$$N_{\theta\theta}^{f} = N_{\theta\theta}^{M} + N_{\theta\theta}^{T} + N_{\theta\theta}^{E}, \tag{37}$$

where $N_{\alpha\alpha}^{M} = N_{\beta\beta}^{M} = 0$ are mechanical forces; $N_{\alpha\alpha}^{E} = 2V_0 e_{32}$, $M_{xx}^{M} = 2V_0 e_{31}$ are electrical forces; $N_{\theta\theta}^{T}, N_{xx}^{T}$ are thermal forces which may be written as

$$\begin{Bmatrix} N_{xx}^{T} \\ N_{\theta\theta}^{T} \end{Bmatrix} = \int_{-h/2}^{h/2} \begin{Bmatrix} C_{11}(T,z)\alpha_{xx}(z) + C_{12}(T,z)\alpha_{\theta\theta}(z) \\ C_{12}(T,z)\alpha_{xx}(z) + C_{22}(T,z)\alpha_{\theta\theta}(z) \end{Bmatrix} \Delta T\, dz, \tag{38}$$

7. Motion equations

The governing equations can be derived by Hamilton's principal as follows

$$\int_0^t (\delta U - \delta K - \delta W - \delta W_e) dt = 0. \tag{39}$$

Substituting Eqs. (25), (31), (32) and (35) into Eq. (39) yields the following governing equations

$$\delta u: \frac{\partial N_{xx}}{\partial x} + \frac{\partial N_{x\theta}}{R\partial\theta} = I_0 \frac{\partial^2 u}{\partial t^2} + I_1 \frac{\partial^2 \phi_x}{\partial t^2}, \tag{40}$$

$$\delta v: \frac{\partial N_{x\theta}}{\partial x} + \frac{\partial N_{\theta\theta}}{R\partial\theta} + \frac{Q_\theta}{R} = I_0 \frac{\partial^2 v}{\partial t^2} + I_1 \frac{\partial^2 \phi_\theta}{\partial t^2}, \tag{41}$$

$$\delta w: \frac{\partial Q_x}{\partial x} + \frac{\partial Q_\theta}{R\partial\theta} - \frac{N_{\theta\theta}}{R} + N_{xx}^{f}\frac{\partial^2 w}{\partial x^2} + N_{\theta\theta}^{f}\frac{\partial^2 w}{R^2\partial\theta^2} - K_w w + K_g \nabla^2 w = I_0 \frac{\partial^2 w}{\partial t^2}, \tag{42}$$

$$\delta \phi_x: \frac{\partial M_{xx}}{\partial x} + \frac{\partial M_{x\theta}}{R\partial\theta} - Q_x = I_2 \frac{\partial^2 \phi_x}{\partial t^2} + I_1 \frac{\partial^2 u}{\partial t^2}, \tag{43}$$

$$\delta \phi_\theta: \frac{\partial M_{x\theta}}{\partial x} + \frac{\partial M_{\theta\theta}}{R\partial\theta} - Q_\theta = I_2 \frac{\partial^2 \phi_\theta}{\partial t^2} + I_1 \frac{\partial^2 v}{\partial t^2}, \tag{44}$$

$$\delta\phi: \int_{-h/2}^{h/2}\left\{\left[\cos\left(\frac{\pi z}{h}\right)\frac{\partial D_x}{\partial x}\right]+\left[\cos\left(\frac{\pi z}{h}\right)\frac{\partial D_\theta}{R\partial\theta}\right]+D_z\left[\frac{\pi}{h}\sin\left(\frac{\pi z}{h}\right)\right]\right\}dz=0 \tag{45}$$

Substituting Eqs. (A1) to (A8) into Eqs. (40) to (45), the governing equations can be obtained as listed in Appendix B. In this paper, three types of boundary conditions are used which are

Simple-Simple (*SS*)

$$x=0,L\Rightarrow u=v=w=\phi_\theta=M_x=0, \tag{46}$$

Clamped- Clamped (*CC*)

$$x=0,L\Rightarrow u=v=w=\phi_x=\phi_\theta=0, \tag{47}$$

Clamped- Simple (*CS*)

$$\begin{aligned} &x=0\Rightarrow u=v=w=\phi_x=\phi_\theta=0,\\ &x=L\Rightarrow u=v=w=\phi_x=M_x=0. \end{aligned} \tag{48}$$

8. Solution procedure

DCM is a numerical procedure expressing a calculus operator ($\Re$) value of the function ($f(x, \theta)$) at a discrete point in the solution domain as a weighted linear sum of discrete function values chosen within the overall domain of a problem. For a two-dimensional problem, supposing that there are N arbitrarily located grid points, the cubature approximation at the ith discrete point can be expressed as (Kolahchi *et al*. 2016a, b)

$$\Re f(x,\theta)_i\approx\sum_{j=1}^{N}C_{ij}f(x_j,\theta_j), \tag{49}$$

where C_{ij} and N are the cubature weighting coefficients and total number of grid points in the solution domain, respectively. The computation of the weighting coefficients can be done using the following expression (Kolahchi *et al*. 2016a, b)

$$\Re\left\{x^{\nu-\mu}\theta^{\mu}\right\}_i=\sum_{j=1}^{N}C_{ij}f(x_j^{\nu-\mu}\theta_j^{\mu}),\ \mu=0,1,2,...,\nu,\ \ \nu=0,1,2,...,N-1,\ \ i=1,2,...,N. \tag{50}$$

The above equation may be written in matrix form as

$$\left[x_j^{\nu-\mu}\theta_j^{\mu}\right]\begin{bmatrix}C_{i1}\\C_{i2}\\\cdot\\\cdot\\\cdot\\C_{in}\end{bmatrix}=\left[\Re\left\{x^{\nu-\mu}\theta^{\mu}\right\}_i\right] \tag{51}$$

The coefficient matrix, $[x_i^{\nu-\mu}\theta_i^{\mu}]$ can be expanded with j in column wise and one row of each pair of (ν, μ). Also, each pair of (ν, μ) is required to fill the column on the right of the equal sign. The cubature weighting coefficients may be obtained by solving Eq. (30) repeatedly for i = 1, 2, ..., N, respectively.

Based on Eqs. (49) and (50), the motion equations (i.e., Eqs. (40) to (45)) may be written in matrix form as follows

$$\left(\underbrace{\begin{bmatrix} K_{bb} & K_{bd} \\ K_{db} & K_{dd} \end{bmatrix}}_{[K]} + \underbrace{\begin{bmatrix} M_{bb} & M_{bd} \\ M_{db} & M_{dd} \end{bmatrix}}_{[M]} \omega^2 \right) \begin{bmatrix} Y_b \\ Y_d \end{bmatrix} = \begin{bmatrix} 0 \\ 0 \end{bmatrix}. \tag{52}$$

where [K] and [M] are stiffness and mass matrixes, respectively; Y is the displacement vector (Y = (u, v, w, ϕ_x, ϕ_θ, ϕ)); subtitles of b and d are related to boundary and domain points, respectively. Finally, for calculating the frequency of the system (ω), the eigenvalue problem can be used.

9. Numerical results and discussion

In this section, the effects of different parameters on the frequency of system are shown. For this purpose, PZT-5A is selected for the piezoelectric cylindrical shell with the following temperature-dependent thermal, mechanical and electrical properties as (Yaqoob Yasin and Kapuria 2014, Shen 2005)

$$E_{11} = E_{110}\left(1 + E_{111}\Delta T\right) \tag{53a}$$

$$E_{22} = E_{220}\left(1 + E_{221}\Delta T\right) \tag{53b}$$

$$E_{33} = E_{330}\left(1 + E_{331}\Delta T\right) \tag{53c}$$

$$G_{12} = G_{120}\left(1 + G_{121}\Delta T\right) \tag{53d}$$

$$G_{13} = G_{130}\left(1 + G_{131}\Delta T\right) \tag{53e}$$

$$G_{23} = G_{230}\left(1 + G_{231}\Delta T\right) \tag{53f}$$

$$\alpha_{xx} = \alpha_{110}\left(1 + \alpha_{111}\Delta T\right) \tag{53g}$$

$$\alpha_{\theta\theta} = \alpha_{220}\left(1 + \alpha_{221}\Delta T\right) \tag{53h}$$

$$e_{31} = d_{31}C_{11} + d_{32}C_{12}, \tag{53i}$$

$$e_{32} = d_{31}C_{12} + d_{32}C_{22}, \tag{53j}$$

$$e_{33} = d_{33}C_{33}, \tag{53k}$$

Table 1 Elastic, piezoelectric and thermal constants of PZT-5

Elastic constants	Piezoelectric constants	Thermal coefficients
$E_{110} = E_{220} = 61\ GPa$ $E_{330} = 53.2\ GPa$ $G_{120} = G_{130} = G_{230} = 24.2\ GPa$ $\upsilon_{12} = 0.35$ $\upsilon_{23} = \upsilon_{13} = 0.38$ $E_{111} = -0.0005$ $E_{221} = E_{331} = G_{121} = G_{131} = G_{231} = -0.0002$	$d_{31} = d_{32} = -1.71\times10^{-10}\ m/V$ $d_{24} = d_{15} = 5.84\times10^{-10}\ m/V$ $d_{33} = 3.74\times10^{-10}\ m/V$	$\alpha_{120} = \alpha_{220} = 0.9\times10^{-6}\ 1/K$ $\alpha_{111} = \alpha_{221} = 0.0005$

Table 2 Temperature-dependent material properties of (10, 10) SWCNT (L = 9.26 nm, R = 0.68 nm, h = 0.067 nm, $\upsilon_{12}^{CNT} = 0.175$) (Shen and Chen 2011)

V_{CNT}	MD (Liew *et al*. 2014)		Rule of mixture			
	$E_{11}(GPa)$	$E_{22}(GPa)$	$E_{11}(GPa)$	η_1	$E_{22}(GPa)$	η_2
0.11	94.8	2.2	94.57	0.149	2.2	0.934
0.14	120.2	2.3	120.09	0.150	2.3	0.942
0.17	145.6	3.5	145.08	0.149	3.5	1.381

Table 3 Comparisons of Young's moduli for PmPV/CNT composites reinforced by (10,10)-tube under T = 300 K (Shen and Chen 2011)

Temperature (K)	$E_{11}^{CNT}(TPa)$	$E_{22}^{CNT}(TPa)$	$G_{12}^{CNT}(TPa)$	$\alpha_{12}^{CNT}(10^{-6}/K)$	$\alpha_{22}^{CNT}(10^{-6}/K)$
300	5.6466	7.0800	1.9445	3.4584	5.1682
500	5.5308	6.9348	1.9643	4.5361	5.0189
700	5.4744	6.8641	1.9644	4.6677	4.8943

$$e_{24} = d_{24}C_{44}, \tag{53l}$$

$$e_{15} = d_{15}C_{55}, \tag{53m}$$

where the above constants are listed in Table 1.

Furthermore, the material properties of CNTs as reinforce and efficiency parameter η_j are shown in Tables 2 and 3, respectively. The Poly dimethylsiloxane (PDMS) is selected for elastomeric medium with v_s = 0.48 and E_s = (3.22 – 0.0034T) GPa in which $T = T_0 + \Delta T$ and T_0 = 300 K (room temperature) (Shen and Chen 2011).

9.1 Convergence of DCM

The convergence and accuracy of the DC method in evaluating the dimensionless frequency of structure is shown in Fig. 2 for different grid point numbers. Fast rate of convergence of the method is quite evident and it is proven that the results may be converged with 113 grid points.

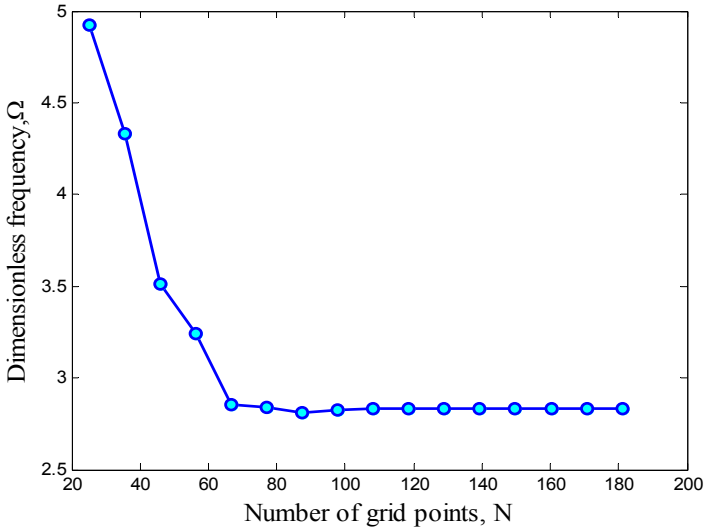

Fig. 2 Convergence and accuracy of DCM

9.2 Validation

In order to validated the results of this work, ignoring the CNT volume percent (i.e., $V_{CNT} = 0$), elastic medium (i.e., $K_w = K_g = 0$) and temperature dependency of shell (i.e., $T = 300\ K$), vibration of a piezoelectric cylindrical shell is investigated. Based on FSDT and Navier's method, the frequency of structure is obtained and compared with the results of Sheng and Wang (2010) in Fig. 3. As can be seen, present results are in good agreement with those reported by Sheng and Wang (2010), indicating validation of present work.

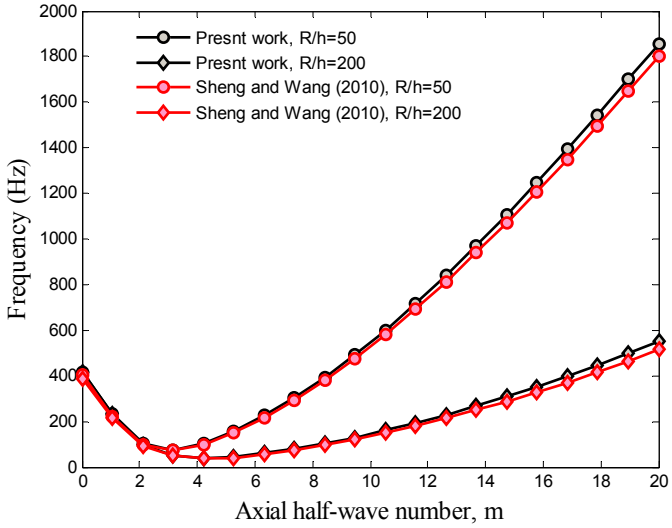

Fig. 3 Comparison of present work with Sheng and Wang (2010)

9.3 Effects of different parameters on vibration of system

The effect of distribution type of CNT in piezoelectric cylindrical shell on the dimensionless frequency $(\Omega = \omega L\sqrt{\rho_m / E_{11}^m})$ of system versus external applied voltage is shown in Fig. 4. The CNT uniform distribution and three types of FG patterns namely as FGV, FGO and FGX are considered. It can be seen that the dimensionless frequency decreases with changing external applied voltage from negative to positive values. In the other words, the dimensionless frequency of structure with applying negative external voltage is higher than the dimensionless frequency of

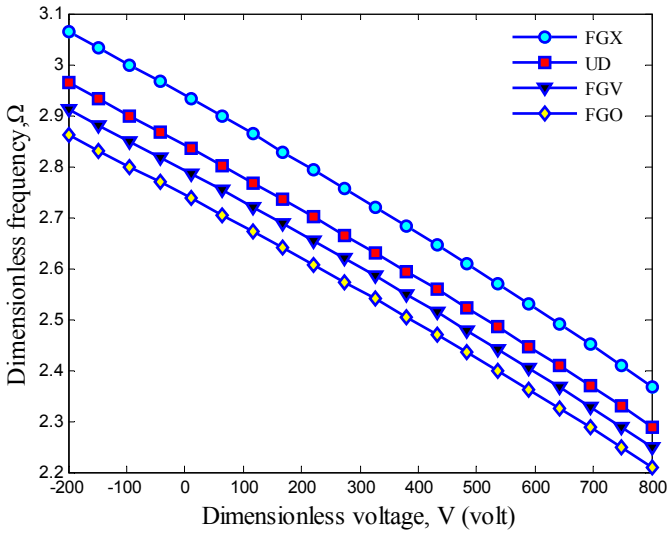

Fig. 4 Dimension frequency versus external applied voltage for different CNT distribution types

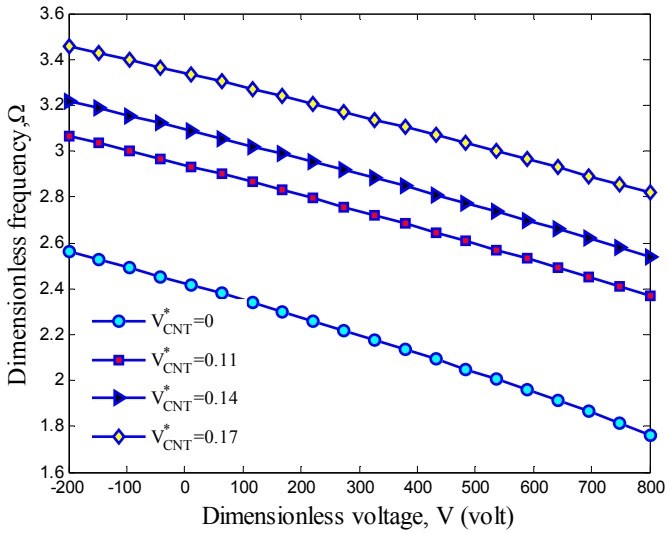

Fig. 5 Dimension frequency versus external applied voltage for different CNT volume percent

structure with applying positive one. It is since the applied positive and negative voltages createthe axial compressive and tensile forces in the structure, respectively. With respect to the distribution types of CNTs in the shell, it can be concluded that the FGX pattern is the best choice compared to other cases. It is because, in the FGX mode, the frequency of structure is maximum which means the stiffness of system is higher with respect to other three patterns. Meanwhile, the frequency of structure with CNT uniform distribution is higher than FGV and FGO models. However, it can be concluded that the CNT distribution close to top and bottom are more efficient than those distributed nearby the mid-plane.

The effect of the CNT volume fraction on the dimensionless frequency of the CNTRC shell

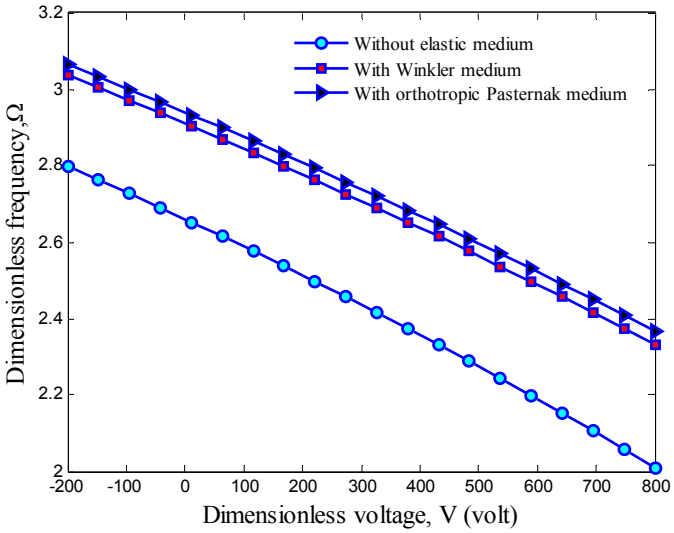

Fig. 6 Dimension frequency versus external applied voltage for different elastic medium types

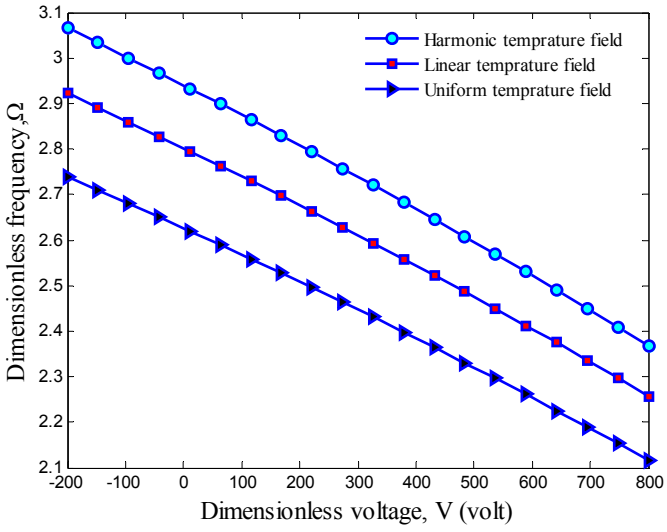

Fig. 7 Dimension frequency versus external applied voltage for different temperature distribution types

with respect to external applied voltage is illustrated in Fig. 5. It can be found that applied negative voltage can increase the dimensionless frequency of the CNTRC shell. It is also observed that increasing the CNT volume fraction increases the dimensionless frequency of structure. This is due to the fact that the increase of CNT volume fraction leads to a harder structure. Hence, applying nanotechnology in shell is a new idea which can harder the system and consequently improve the vibration behavior of structure.

The effect of the temperature-dependent elastic medium type on the dimensionless frequency of the CNTRC shell with respect to applied external voltage is illustrated in Fig. 6. Three cases are considered as without elastic medium ($K_w = 0$ N/m^3, $K_g = 0$ N/m), Winkler medium ($K_w \neq 0$ N/m^3,

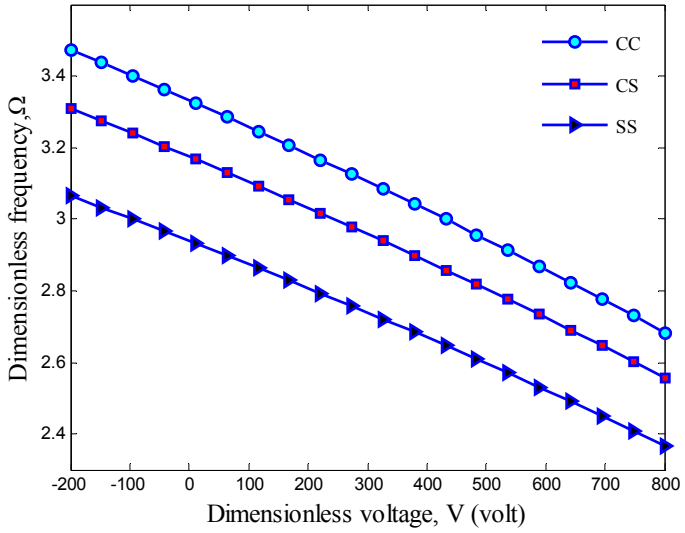

Fig. 8 Dimension frequency versus external applied voltage for different boundary conditions

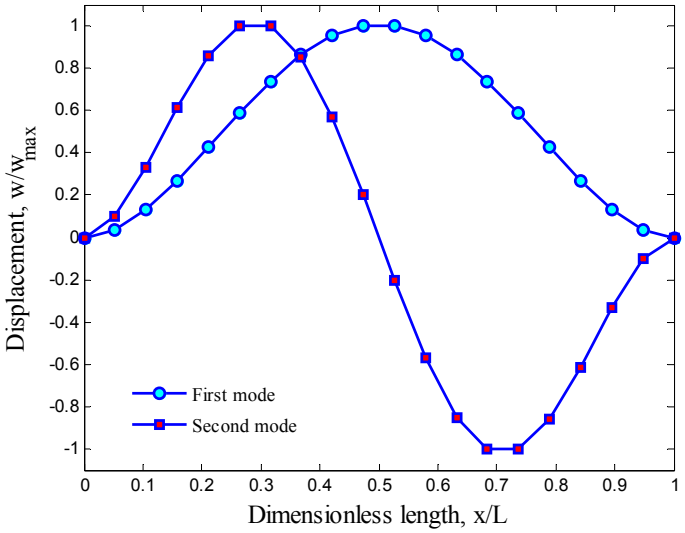

Fig. 9 First and second mode shapes of structure with CC boundary condition

$K_g = 0$ N/m) and Pasternak medium ($K_w \neq 0$ N/m^3, $K_g \neq 0$ N/m). As can be seen, considering elastic medium increases dimensionless frequency of the CNTRC shell. It is due to the fact that considering elastic medium leads to stiffer structure. Furthermore, the effect of the Pasternak-type is higher than the Winkler-type on the dimensionless frequency of the CNTRC shell. It is perhaps due to the fact that the Winkler-type is capable to describe just normal load of the elastic medium while the Pasternak-type describes both transverse shear and normal loads of the elastic medium.

The effect of the temperature distribution type on the dimensionless frequency of the FG-CNT reinforced piezoelectric cylindrical shell is demonstrated in Fig. 7 versus applied external voltage. Here, three cases of uniform, linear and harmonic distribution fields are considered. As can be seen,

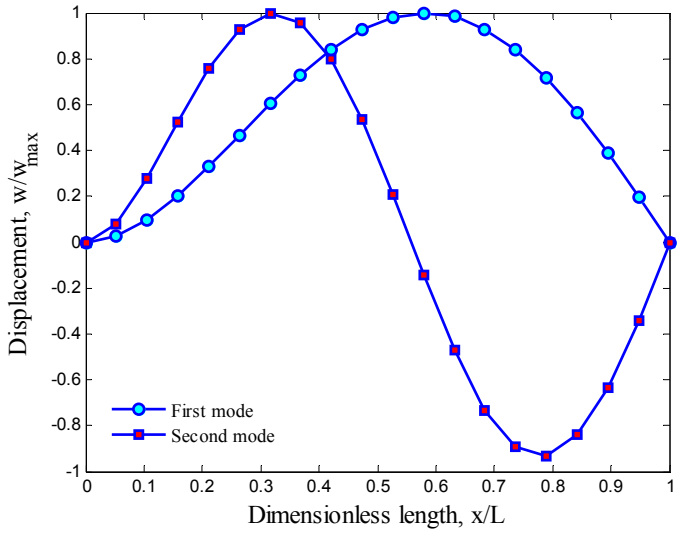

Fig. 10 First and second mode shapes of structure with CS boundary condition

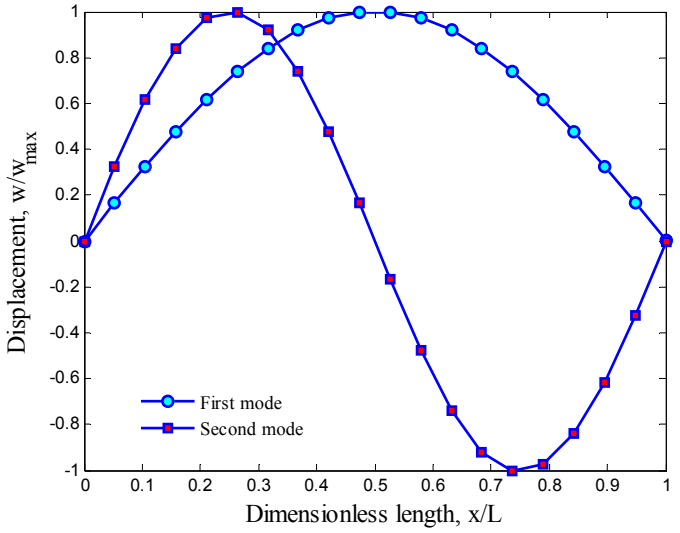

Fig. 11 First and second mode shapes of structure with SS boundary condition

the dimensionless frequency of structure subjected to harmonic temperature field is higher than linear and uniform ones. In addition, the non-uniform temperature distributions lead to higher frequency with respect to the structure under uniform temperature field.

The effect of different boundary conditions on the dimensionless frequency of system against external applied voltage is plotted in Fig. 8. As can be seen, the structure with CC boundary condition has maximum dimensionless frequency with respect to other cases. It is due to the fact that the CC boundary condition makes the structure harder. Furthermore, the dimensionless frequency of cylindrical shell with the assumed boundary conditions follows the below order:

CC > CS > SS.

The mode shapes of the structure for the first and second modes are shown in Figs. 9-11, respectively for CC, CS and SS boundary conditions. It can be seen that the boundary conditions are satisfied at both ends of the cylindrical shell. Furthermore, the maximum deflection of FG-CNT reinforced cylindrical shell for CC and SS boundary conditions is happen at the middle of structure while for CS boundary condition, it is near the right side of cylindrical shell.

10. Conclusions

Temperature-dependent vibration analysis of FG-CNT-reinforced piezoelectric cylindrical shell subjected to uniform and non-uniform temperature distributions was presented in this study. The structure was subjected to external voltage in the thickness direction. The Mixture rule is used for obtaining the material properties of structure. The surrounding elastic medium was simulated by temperature-dependent Pasternak foundation. Utilizing FSDT, energy method and Hamilton's principle, the motion equations were derived. DC method was used for calculating the frequency of structure for different boundary conditions. The effects of the external applied voltage, volume percent and distribution type of CNT in polymer, temperature distribution type, elastic medium and boundary conditions on the frequency of system were shown. The results indicate that the dimensionless frequency decreases with changing external applied voltage from negative to positive values. It can be concluded that the FGX pattern is the best choice compared to other cases. The frequency of structure with CNT uniform distribution was higher than FGV and FGO models. It was also observed that increasing the CNT volume fraction increases the dimensionless frequency of structure. In addition, considering elastic medium increases the dimensionless frequency of the CNTRC shell. With respect to the effect of temperature distribution type, the dimensionless frequency of structure subjected to harmonic temperature field was higher than linear and uniform ones. Furthermore, the structure with CC boundary condition has higher dimensionless frequency with respect to SS and CS one. Present results were validated with those reported by Sheng and Wang (2010). Finally, it is hoped that the results presented in this paper would be helpful for control and design of NEMS/MEMS devices such as strain sensor, mass and pressure sensors.

References

Alibeigloo, A. (2013), "Static analysis of functionally graded carbon nanotube-reinforced composite plate embedded in piezoelectric layers by using theory of elasticity", *Compos. Struct.*, **95**, 612-622.

Alibeigloo, A. and Nouri, V. (2010), "Static analysis of functionally graded cylindrical shell with

piezoelectric layers using differential quadrature method", *Compos*. *Struct*., **92**(8), 1775-1785.
Bodaghi, M. and Shakeri, M. (2012), "An analytical approach for free vibration and transient response of functionally graded piezoelectric cylindrical panels subjected to impulsive loads", *Compos*. *Struct*., **94**(5), 1721-1735.
Jinhua, Y., Jie, Y. and Kitipornchai, S. (2013), "Dynamic stability of piezoelectric laminated cylindrical shells with delamination", *J*. *Intel*. *Mater*. *Syst*. *Struct*., **24**, 1770-1781.
Kolahchi, R., Safari, M. and Esmailpour, M. (2016a), "Dynamic stability analysis of temperature-dependent functionally graded CNT-reinforced visco-plates resting on orthotropic elastomeric medium", *Compos*. *Struct*., **150**, 255-265.
Kolahchi, R., Hosseini, H. and Esmailpour, M. (2016b), "Differential cubature and quadrature-Bolotin methods for dynamic stability of embedded piezoelectric nanoplates based on visco-nonlocal-piezoelasticity theories", *Compos*. *Struct*., **157**, 174-186.
Lei, Z.X., Zhang, L.W., Liew, K.M. and Yu, J.L. (2014), "Dynamic stability analysis of carbonnanotube-reinforced functionally graded cylindrical panels using the element-free kp-Ritz method", *Compos*. *Struct*., **113**, 328-338,.
Lei, Z.X., Zhang, L.W. and Liew, K.M. (2015a), "Free vibration analysis of laminated FG-CNT reinforced composite rectangular plates using the kp-Ritz method", *Compos*. *Struct*., **127**, 245-259.
Lei, Z.X., Zhang, L.W. and Liew, K.M. (2015b), "Elastodynamic analysis of carbon nanotube-reinforced functionally graded plates", *Int*. *J*. *Mech*. *Sci*., **99**, 208-217.
Lei, Z.X., Zhang, L.W. and Liew, K.M. (2016), "Analysis of laminated CNT reinforced functionally graded plates using the element-free kp-Ritz method", *Compos*. *Part B*: *Eng*., **84**, 211-221.
Liew, K.M., Lei, Z.X., Yu, J.L. and Zhang, L.W. (2014), "Postbuckling of carbon nanotube-reinforced functionally graded cylindrical panels under axial compression using a meshless approach", *Comput*. *Methods Appl*. *Mech*. *Eng*., **268**, 1-17.
Liu, C., Ke, L.L., Wang, Y.S., Yang, J. and Kitipornchai, S. (2013), "Thermo-electromechanical vibration of piezoelectric nanoplates based on the nonlocal theory", *Compos*. *Struct*., **106**, 167-174.
Nanda, N. and Nath, Y. (2012), "Active control of delaminated composite shells with piezoelectric sensor/actuator patches", *Struct*. *Eng*. *Mech*., *Int*. *J*., **42**(2), 211-228.
Rajesh Bhangale, K. and Ganesan, N. (2005), "Free vibration studies of simply supported non-homogeneous functionally graded magneto- electro-elastic finite cylindrical shells", *J*. *Sound Vib*., **23**(1-2), 412-422.
Reddy, J.N. (2002), *Mechanics of Laminated Composite Plates and Shells*: *Theory and Analysis*, Second Edition, CRC Press.
Shen, H. (2005), "Postbuckling of FGM plates with piezoelectric actuators under thermo-electro-mechanical loadings", *Int*. *J*. *Solids Struct*., **42**(23), 6101-6121.
Shen, H. (2009), "Nonlinear bending of functionally graded carbon nanotube-reinforced composite plates in thermal environments", *Compos*. *Struct*., **91**(1), 9-19.
Shen, H. and Chen, Zh. (2011), "Nonlocal beam model for nonlinear analysis of carbon nanotubes on elastomeric substrates", *Comput*. *Mat*. *Sci*., **50**(3), 1022-1029.
Sheng, G.G. and Wang, X. (2009a), "Active control of functionally graded laminated cylindrical shells", *Compos*. *Struct*., **90**(4), 448-457.
Sheng, G.G. and Wang, X. (2009b), "Studies on dynamic behavior of functionally graded cylindrical shells with PZT layers under moving loads", *J*. *Sound Vib*., **323**(3-5), 772-789.
Sheng, G.G. and Wang, X. (2010), "Thermoelastic vibration and buckling analysis of functionally graded piezoelectric cylindrical shells", *Appl*. *Math*. *Model*., **34**(9), 2630-2643.
Tiersten, H.F. (1969), "Linear Piezoelectric Plate Vibrations", Plenum Press, New York.
Yaqoob Yasin, M. and Kapuria, S. (2014), "An efficient finite element with layerwise mechanics for smart piezoelectric composite and sandwich shallow shells", *Comput*. *Mech*., **53**(1), 101-124.
Zhang, L.W. and Liew, K.M. (2015a), "Large deflection analysis of FG-CNT reinforced composite skew plates resting on Pasternak foundations using an element-free approach", *Compos*. *Struct*., **132**, 974-993.
Zhang, L.W. and Liew, K.M. (2015b), "Geometrically nonlinear large deformation analysis of functionally

graded carbon nanotube reinforced composite straight-sided quadrilateral plates", *Comput. Meth. Appl. Mech. Eng.*, **295**, 219-239.
Zhang, L.W. and Liew, K.M. (2016a), "Element-free geometrically nonlinear analysis of quadrilateral functionally graded material plates with internal column supports", *Compos. Struct.*, **147**, 99-110.
Zhang, L.W. and Liew, K.M. (2016b), "Postbuckling analysis of axially compressed CNT reinforced functionally graded composite plates resting on Pasternak foundations using an element-free approach", *Compos. Struct.*, **138**, 40-51.
Zhang, L.W., Zhu, P. and Liew, K.M. (2014a), "Thermal buckling of functionally graded plates using a local Kriging meshless method", *Compos. Struct.*, **108**, 472-492.
Zhang, L.W., Lei, Z.X., Liew, K.M. and Yu, J.L. (2014b), "Large deflection geometrically nonlinear analysis of carbon nanotube-reinforced functionally graded cylindrical panels", *Comput. Methods Appl. Mech. Eng.*, **273**, 1-18.
Zhang, L.W., Lei, Z.X., Liew, K.M. and Yu, J.L. (2014c), "Static and dynamic of carbon nanotube reinforced functionally graded cylindrical panels", *Compos. Struct.*, **111**, 205-212,.
Zhang, L.W., Li, D.M. and Liew, K.M. (2015a), "An element-free computational framework for elastodynamic problems based on the IMLS-Ritz method", *Eng. Anal. Bound. Elem.*, **54**, 39-46.
Zhang, L.W., Huang, D. and Liew, K.M. (2015b), "An element-free IMLS-Ritz method for numerical solution of three-dimensional wave equations", *Comput. Meth. Appl. Mech. Eng.*, **297**, 116-139.
Zhang, Sh., Schmidt, R. and Qin, X. (2015c), "Active vibration control of piezoelectric bonded smart structures using PID algorithm", *Chin. J. Aero.*, **28**(1), 305-313.
Zhang, L.W., Song, Z.G. and Liew, K.M. (2015d), "State-space Levy method for vibration analysis of FG-CNT composite plates subjected to in-plane loads based on higher-order shear deformation", *Compos. Struct.*, **134**, 989-1003.
Zhang, L.W., Lei, Z.X. and Liew, K.M. (2015e), "Buckling analysis of FG-CNT reinforced composite thick skew plates using an element-free approach", *Compos. Part B: Eng.*, **75**, 36-46.
Zhang, L.W., Song, Z.G. and Liew, K.M. (2015f), "Nonlinear bending analysis of FG-CNT reinforced composite thick plates resting on Pasternak foundations using the element-free IMLS-Ritz method", *Compos. Struct.*, **128**, 165-175.
Zhang, L.W., Cui, W.C. and Liew, K.M. (2015g), "Vibration analysis of functionally graded carbon nanotube reinforced composite thick plates with elastically restrained edges", *Int. J. Mech. Sci.*, **103**, 9-21.
Zhang, L.W., Lei, Z.X. and Liew, K.M. (2015h), "Free vibration analysis of functionally graded carbon nanotube-reinforced composite triangular plates using the FSDT and element-free IMLS-Ritz method", *Compos. Struct.*, **120**, 189-199.
Zhang, L.W., Liew, K.M. and Jiang, Z. (2016a), "An element-free analysis of CNT-reinforced composite plates with column supports and elastically restrained edges under large deformation", *Compos. Part B: Eng.*, **95**, 18-28.
Zhang, L.W., Liew, K.M. and Reddy, J.N. (2016b), "Postbuckling behavior of bi-axially compressed arbitrarily straight-sided quadrilateral functionally graded material plates", *Comput. Meth. Appl. Mech. Eng.*, **300**, 593-610.
Zhang, L.W., Liew, K.M. and Reddy, J.N. (2016c), "Postbuckling of carbon nanotube reinforced functionally graded plates with edges elastically restrained against translation and rotation under axial compression", *Comput. Meth. Appl. Mech. Eng.*, **298**, 1-28.
Zhang, L.W., Liew, K.M. and Reddy, J.N. (2016d), "Postbuckling analysis of bi-axially compressed laminated nanocomposite plates using the first-order shear deformation theory", *Compos. Struct.*, **152**, 418-431.
Zhang, L.W., Song, Z.G. and Liew, K.M. (2016e), "Computation of aerothermoelastic properties and active flutter control of CNT reinforced functionally graded composite panels in supersonic airflow", *Comput. Meth. Appl. Mech. Eng.*, **300**, 427-441.
Zhang, L.W., Song, Z.G. and Liew, K.M. (2016f), "Optimal shape control of CNT reinforced functionally graded composite plates using piezoelectric patches", *Compos. Part B: Eng.*, **85**, 140-149.
Zhang, L.W., Xiao, L.N., Zou, G.L. and Liew, K.M. (2016g), "Elastodynamic analysis of quadrilateral

CNT-reinforced functionally graded composite plates using FSDT element-free method", *Compos*. *Struct*., **148**, 144-154.

Zhang, L.W., Zhang, Y., Zou, G.L. and Liew, K.M. (2016h), "Free vibration analysis of triangular CNT-reinforced composite plates subjected to in-plane stresses using FSDT element-free method", *Compos*. *Struct*., **149**, 247-260.

Zhu, P., Zhang, L.W. and Liew, K.M. (2014), "Geometrically nonlinear thermomechanical analysis of moderately thick functionally graded plates using a local Petrov–Galerkin approach with moving Kriging interpolation", *Compos*. *Struct*., **107**, 298-314.

CC

Appendix A

$$N_{xx} = A_{110}\frac{\partial u}{\partial x} + A_{111}\frac{\partial \phi_x}{\partial x} + A_{120}\left(\frac{\partial v}{R\partial\theta} + \frac{w}{R}\right) + A_{121}\frac{\partial \phi_\theta}{R\partial\theta} + E_{31}\phi, \tag{A1}$$

$$N_{\theta\theta} = A_{120}\frac{\partial u}{\partial x} + A_{121}\frac{\partial \phi_x}{\partial x} + A_{220}\left(\frac{\partial v}{R\partial\theta} + \frac{w}{R}\right) + A_{221}\frac{\partial \phi_\theta}{R\partial\theta} + E_{32}\phi, \tag{A2}$$

$$Q_\theta = k^{'}A_{44}\left[\frac{1}{R}\left(\frac{\partial w}{\partial\theta} - v\right) + \phi_\theta\right] + E_{15}\frac{\partial \phi}{R\partial\theta}, \tag{A3}$$

$$Q_x = k^{'}A_{55}\left(\frac{\partial w}{\partial x} + \phi_x\right) + E_{24}\frac{\partial \phi}{\partial x}, \tag{A4}$$

$$N_{x\theta} = A_{660}\left(\frac{\partial u}{R\partial\theta} + \frac{\partial v}{\partial x}\right) + A_{661}\left(\frac{\partial \phi_x}{R\partial\theta} + \frac{\partial \phi_\theta}{\partial x}\right), \tag{A5}$$

$$M_{xx} = A_{111}\frac{\partial u}{\partial x} + A_{112}\frac{\partial \phi_x}{\partial x} + A_{121}\left(\frac{\partial v}{R\partial\theta} + \frac{w}{R}\right) + A_{122}\frac{\partial \phi_\theta}{R\partial\theta} + F_{31}\phi, \tag{A6}$$

$$M_{\theta\theta} = A_{121}\frac{\partial u}{\partial x} + A_{122}\frac{\partial \phi_x}{\partial x} + A_{221}\left(\frac{\partial v}{R\partial\theta} + \frac{w}{R}\right) + A_{222}\frac{\partial \phi_\theta}{R\partial\theta} + F_{32}\phi, \tag{A7}$$

$$M_{x\theta} = A_{661}\left(\frac{\partial u}{R\partial\theta} + \frac{\partial v}{\partial x}\right) + A_{662}\left(\frac{\partial \phi_x}{R\partial\theta} + \frac{\partial \phi_\theta}{\partial x}\right), \tag{A8}$$

where

$$A_{11k} = \int_{-h/2}^{h/2} C_{11} z^k dz, \qquad k = 0,1,2 \tag{A9}$$

$$A_{12k} = \int_{-h/2}^{h/2} C_{12} z^k dz, \qquad k = 0,1,2 \tag{A10}$$

$$A_{22k} = \int_{-h/2}^{h/2} C_{22} z^k dz, \qquad k = 0,1,2 \tag{A11}$$

$$A_{66k} = \int_{-h/2}^{h/2} C_{66} z^k dz, \qquad k = 0,1,2 \tag{A12}$$

$$A_{44} = \int_{-h/2}^{h/2} C_{44} dz, \tag{A13}$$

$$A_{55} = \int_{-h/2}^{h/2} C_{55} z^k dz, \tag{A14}$$

$$\left(E_{31}, E_{32}\right) = \frac{\pi}{h} \int_{-h/2}^{h/2} \left(e_{31}, e_{32}\right) \sin\left(\frac{\pi z}{h}\right) dz, \tag{A15}$$

$$\left(E_{24}, E_{15}\right) = -\int_{-h/2}^{h/2} \left(e_{24}, e_{15}\right) \cos\left(\frac{\pi z}{h}\right) dz, \tag{A16}$$

$$\left(F_{31}, F_{32}\right) = \frac{\pi}{h} \int_{-h/2}^{h/2} \left(e_{31}, e_{32}\right) \sin\left(\frac{\pi z}{h}\right) z dz, \tag{A17}$$

Appendix B

$$\begin{aligned} &A_{110}\frac{\partial^2 u}{\partial x^2} + A_{111}\frac{\partial^2 \phi_x}{\partial x^2} + A_{120}\left(\frac{\partial^2 v}{R\partial\theta\partial x} + \frac{1}{R}\frac{\partial w}{\partial x}\right) + A_{121}\frac{\partial^2 \phi_\theta}{R\partial\theta\partial x} + E_{31}\frac{\partial \phi}{\partial x} \\ &+ A_{120}\frac{\partial^2 u}{R\partial x\partial\theta} + A_{121}\frac{\partial^2 \phi_x}{R\partial x\partial\theta} + A_{220}\left(\frac{\partial^2 v}{R^2\partial\theta^2} + \frac{1}{R^2}\frac{\partial w}{\partial\theta}\right) + A_{221}\frac{\partial^2 \phi_\theta}{R^2\partial\theta^2} \\ &+ E_{32}\frac{\partial \phi}{\partial\theta} = I_0\frac{\partial^2 u}{\partial t^2} + I_1\frac{\partial^2 \phi_x}{\partial t^2}, \end{aligned} \tag{B1}$$

$$\begin{aligned} &A_{120}\frac{\partial^2 u}{R\partial x\partial\theta} + A_{121}\frac{\partial^2 \phi_x}{R\partial x\partial\theta} + A_{220}\left(\frac{\partial^2 v}{R^2\partial\theta^2} + \frac{1}{R^2}\frac{\partial w}{\partial\theta}\right) + A_{221}\frac{\partial^2 \phi_\theta}{R^2\partial\theta^2} \\ &+ \frac{E_{32}}{R}\frac{\partial \phi}{\partial\theta} + A_{660}\left(\frac{\partial^2 u}{R\partial\theta\partial x} + \frac{\partial^2 v}{\partial x^2}\right) + A_{661}\left(\frac{\partial^2 \phi_x}{R\partial\theta\partial x} + \frac{\partial^2 \phi_\theta}{\partial x^2}\right) \\ &= I_0\frac{\partial^2 v}{\partial t^2} + I_1\frac{\partial^2 \phi_\theta}{\partial t^2}, \end{aligned} \tag{B2}$$

$$
\begin{aligned}
&k^{'}A_{44}\left[\frac{1}{R^2}\left(\frac{\partial w}{\partial\theta^2}-\frac{\partial v}{\partial\theta}\right)+\frac{1}{R}\frac{\partial\phi_\theta}{\partial\theta}\right]+E_{15}\frac{\partial\phi}{R^2\partial\theta^2}+k^{'}A_{55}\left(\frac{\partial^2 w}{\partial x^2}+\frac{\partial\phi_x}{\partial x}\right)\\
&+E_{24}\frac{\partial^2\phi}{\partial x^2}-A_{120}\frac{\partial u}{\partial x}-A_{121}\frac{\partial\phi_x}{\partial x}-A_{220}\left(\frac{\partial v}{R\partial\theta}+\frac{w}{R}\right)-A_{221}\frac{\partial\phi_\theta}{R\partial\theta},\\
&N_{xx}^{f}\frac{\partial^2 w}{\partial x^2}+N_{\theta\theta}^{f}\frac{\partial^2 w}{R^2\partial\theta^2}-K_w w+K_g\nabla^2 w=I_0\frac{\partial^2 w}{\partial t^2},
\end{aligned}
\tag{B3}
$$

$$
\begin{aligned}
&A_{111}\frac{\partial^2 u}{\partial x^2}+A_{112}\frac{\partial^2\phi_x}{\partial x^2}+A_{121}\left(\frac{\partial^2 v}{R\partial\theta\partial x}+\frac{1}{R}\frac{\partial w}{\partial x}\right)+A_{122}\frac{\partial^2\phi_\theta}{R\partial\theta}+F_{31}\frac{\partial\phi}{\partial x}+\\
&A_{661}\left(\frac{\partial^2 u}{R^2\partial\theta^2}+\frac{\partial^2 v}{R\partial x\partial\theta}\right)+A_{662}\left(\frac{\partial^2\phi_x}{R^2\partial\theta^2}+\frac{\partial^2\phi_\theta}{R\partial x\partial\theta}\right)-k^{'}A_{55}\left(\frac{\partial w}{\partial x}+\phi_x\right)\\
&-E_{24}\frac{\partial\phi}{\partial x}=I_2\frac{\partial^2\phi_x}{\partial t^2}+I_1\frac{\partial^2 u}{\partial t^2},
\end{aligned}
\tag{B4}
$$

$$
\begin{aligned}
&A_{121}\frac{\partial^2 u}{R\partial x\partial\theta}+A_{122}\frac{\partial^2\phi_x}{R\partial x\partial\theta}+A_{221}\left(\frac{\partial^2 v}{R^2\partial\theta^2}+\frac{1}{R^2}\frac{\partial w}{\partial\theta}\right)+A_{222}\frac{\partial^2\phi_\theta}{R^2\partial\theta^2}\\
&+\frac{F_{32}}{R}\frac{\partial\phi}{\partial\theta}+A_{661}\left(\frac{\partial^2 u}{R\partial\theta\partial x}+\frac{\partial^2 v}{\partial x^2}\right)+A_{662}\left(\frac{\partial^2\phi_x}{R\partial\theta\partial x}+\frac{\partial^2\phi_\theta}{\partial x^2}\right)\\
&-k^{'}A_{44}\left[\frac{1}{R}\left(\frac{\partial w}{\partial\theta}-v\right)+\phi_\theta\right]-E_{15}\frac{\partial\phi}{R\partial\theta}=I_2\frac{\partial^2\phi_\theta}{\partial t^2}+I_1\frac{\partial^2 v}{\partial t^2},
\end{aligned}
\tag{B5}
$$

$$
\begin{aligned}
&\delta\phi:\quad -E_{15}\left(\frac{\partial\phi_x}{\partial x}+\frac{\partial^2 w}{\partial x^2}\right)+\Xi_{11}\left(\frac{\partial^2\varphi}{R\partial x\partial\theta}\right)-E_{24}\left(\frac{1}{R^2}\left(\frac{\partial^2 w}{\partial\theta^2}-\frac{\partial v}{\partial\theta}\right)+\frac{\partial\phi_\theta}{R\partial\theta}\right)\\
&+\Xi_{22}\left(\frac{\partial^2\varphi}{R^2\partial\theta^2}\right)+E_{31}\frac{\partial u}{\partial x}+F_{31}\frac{\partial\phi_x}{\partial x}+\frac{E_{32}}{R}\left(w+\frac{\partial v}{\partial\theta}\right)+\frac{F_{32}}{R}\frac{\partial\phi_\theta}{\partial\theta}-\Xi_{33}\varphi=0.
\end{aligned}
\tag{B6}
$$

where

$$
\left(\Xi_{11},\Xi_{22}\right)=\int_{-h/2}^{h/2}\left(\in_{11},\in_{22}\right)\cos^2\left(\frac{\pi z}{h}\right)dz,
\tag{B7}
$$

$$
\left(\Xi_{33}\right)=\frac{\pi^2}{h^2}\int_{-h/2}^{h/2}\left(\in_{33}\right)\sin^2\left(\frac{\pi z}{h}\right)dz.
\tag{B8}
$$